Far-infrared and capacitance measurements of electrons on liquid helium

D. K. Lambert* and P. L. Richards
Department of Physics, University of California, Berkeley, California 94720
and Materials and Molecular Research Division, Lawrence Berkeley Laboratory, Berkeley, California 94720
(Received 8 August 1980)

We have used the techniques of far-infrared laser spectroscopy to study transitions of electrons between bound states in the potential well near a liquid-helium surface. Data measured as a function of surface charge density are used to deduce the local positional disorder of the surface electrons as was reported in a recent Letter. Measurements at low surface charge density and high electric fields are compared with models of the liquid-gas interface. Capacitance measurements and electrostatic calculations provide an accurate determination of the surface charge density and the applied electric field. These calculations show that the charge only covers part of the liquid surface.

I. INTRODUCTION

Electrons in image potential induced states above the surface of liquid-helium provide both a model system[1] for the two-dimensional (2D) electron gas and a probe[2] of the helium liquid-vapor interface. In a recent Letter[3] we gave a preliminary discussion of an experiment which measured the local disorder in a 2D electron gas. We have also measured the transition frequencies between bound states of electrons on the surface using electric field normal to the surface which were much larger than those previously used.[2,4] These measurements are interpreted to provide information about the helium liquid-vapor interface.

In addition to obtaining information about helium surface electrons on the microscopic scale we have used capacitance measurements as a function of cell voltage (CV measurements) and electrostatic calculations to determine the macroscopic static distribution of charge on the surface. An interesting situation analogous to a phase separation in the electron fluid is found. Accurate values of the surface charge density and the electric field acting on the surface electrons are obtained.

This paper is organized as follows: In Sec. II we give a theoretical description of the novel CV technique that allows us to obtain the surface charge density distribution and the electric field acting on surface electrons. In Sec. III we describe the spectroscopic techniques. In Sec. IV we discuss the results of our measurements of the transition frequencies as a function of surface charge density and applied electric field.

II. ANALYSIS OF CV MEASUREMENTS

We have used CV measurements to obtain both the surface charge density as a function of position on the surface and the electric field acting on surface electrons. The electrodes shown in Fig. 1, which were used to confine the surface charge and to make the capacitance measurements, have essentially axial symmetry. The cell has radius a and height h. A gap $s = 0.0215$ cm separates the bottom plate from the grounded cell body. The top plate is separated from the cell body by a 0.084-cm gap. We neglect the width of this gap and use the average of the actual top plate radius and the radius of the hole containing it as the top plate radius b in our analysis. The cell is filled to a depth d with liquid helium as measured by the change in ac capacitance between the top and bottom plates before and after condensing liquid into the cell. A positive potential relative to ground (henceforth called the cell voltage V) is applied to the bottom plate. The fringing electric field from the cell walls confines charge placed on the liquid surface. Free surface charge distributes itself so that the electric field acting on it is normal to the surface.

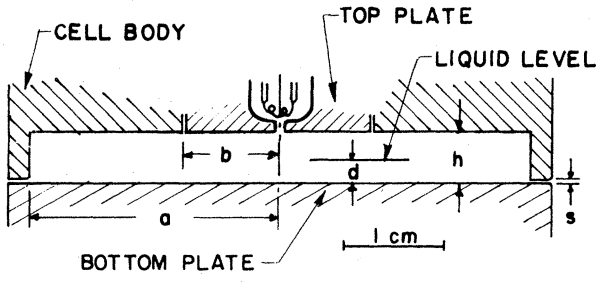

FIG. 1. Cross section of the cylindrical cell used to confine electrons on the helium surface and as an optical cavity for the spectroscopic measurements.

Free charge is deposited on the surface by briefly heating a thoriated tungsten filament above a small hole in the center of the top plate. Afterwards, the measured ac capacitance is found to be a function of the cell voltage V. The measured change of the ac capacitance from the value found with no charge on the surface is shown in Fig. 2 as a function of V. The curve is reversible as long as the cell voltage V is kept above a minimum value. If V is reduced further, the slope of the curve abruptly changes sign. If the voltage is again increased it is found that the ac capacitance follows a new reversible curve above the new minimum voltage.

The average thermal kinetic energy of an electron moving along the surface ($\sim 10^{-4}$ eV at 1 K) is much less than the typical electrical potential energy differences along the surface (~ 1 V). Hence, we can neglect the slight fuzzing caused by thermal motion of the electrons and use electrostatics to calculate the surface charge distribution. The surface is divided into two regions. One region is a circular charge pool centered on the cell axis. The electrical potential is constant over the surface within this charge pool. The other region is an annular ring between the charge pool and the walls of the cell which (in our approximation) contains no charge. The discontinuity in slope of the CV curve occurs when V is reduced to the point at which the charge pool touches the edges of the cell and charge begins to flow off the bulk liquid surface onto the helium film covering the metal walls. Most of the charge that flows onto the walls does not return to the bulk liquid surface when V is again increased.

We have used CV measurements in the reversible region of the curve to obtain both the surface charge density distribution and the electric field acting on electrons near the center of the charge pool as a function of V. Doing so requires a calculation of the electrostatics of the cell when the liquid surface is partially covered with charge. We begin by calculating the surface charge density σ as a function of charge pool radius r, bottom plate voltage V, and top plate voltage V'. The linear relationship between the surface charge density distribution and total charge induced on the bottom plate by the surface charge is also obtained. Finally, these results are used to obtain the change in induced charge on the bottom plate divided by the change in top plate voltage V'. This result divided by the geometrical capacitance with no charge on the surface is the fractional change in ac capacitance $\Delta C/C$, as a function of charge pool radius r and cell voltage V. Because of the linearity

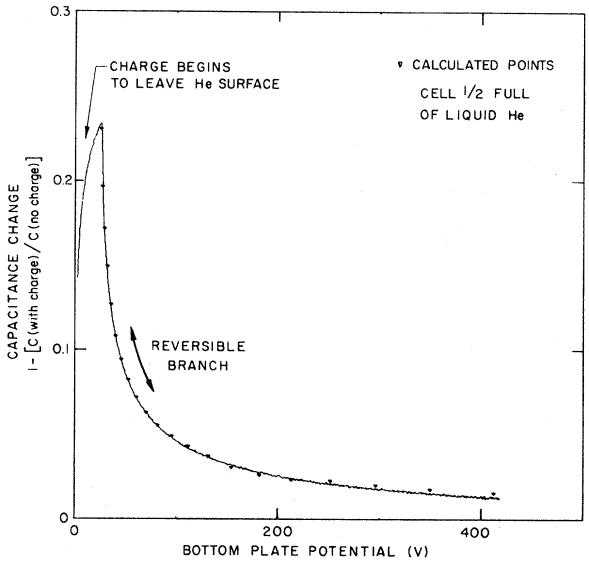

FIG. 2. Comparison between the measured curve of capacitance change vs cell voltage and the result of our electrostatic calculation. The discontinuity in slope occurs when the charge pool begins to flow off the surface onto the walls.

of electrostatics, if V and σ are multiplied by the same factor, the resulting configuration is another solution. Letting V_0 be the cell voltage at which the discontinuity in slope of the CV curve occurs, this implies that $\Delta C/C$ is a function of V and V_0 only through V/V_0. Also, the surface charge density at a given $\Delta C/C$ is proportional to V_0.

Even though we chose the simplest possible geometry, the complicated boundary condition made it necessary to use numerical methods. For purpose of analysis the surface charge is separated into concentric annular rings extending out to the charge pool radius r. The potentials on the bottom plate V and on the top plate V' are specified. The electric field along the surface acting on each ring in the charge pool must be zero. This gives a system of linear equations with a unique solution for the surface charge density in each ring.

The electric field acting on the ith ring is found using the principle of superposition. The radial electric field from the bottom plate at radius ρ on the surface is

$$E_r^{\text{bot}}(\rho) = -\frac{2V}{h} \sum_{n=1}^{\infty} \frac{\sin(n\pi s/h)\sin(n\pi d/h) I_1(n\pi\rho/h)}{(n\pi s/h) I_0(n\pi a/h)} \quad . \tag{1}$$

Here $I_0(x)$ and $I_1(x)$ are modified Bessel functions. The radial electric field from the top plate potential is

$$E_r^{\text{top}}(\rho) = \frac{2bV'}{a^2} \sum_{n=1}^{\infty} \frac{\sinh(x_n d/a) J_1(x_n b/a) J_1(x_n \rho/a)}{\sinh(x_n h/a) J_1^2(x_n)} \quad . \tag{2}$$

Here $J_1(x)$ is the ordinary Bessel function of order unity, and x_n is the nth zero of the ordinary Bessel function of order zero. The radial electric field at a ring of radius ρ_i from a ring with charge density σ_j, width Δr, and radius ρ_j is obtained using the Green's function of a point charge in cylindrical coordinates. For $\rho_i < \rho_j$ we find

$$E_r^{i<j}(\rho_i, \rho_j) = \frac{8\pi^2(\Delta r)\rho_j \sigma_j}{h^2} \sum_{n=1}^{\infty} n R_0\left(\frac{n\pi}{h}, a, \rho_j\right) I_1\left(\frac{n\pi\rho_i}{h}\right) \sin^2\left(\frac{n\pi d}{h}\right) \quad . \tag{3}$$

Here

$$R_0(k,x,y) = K_0(kx) I_0(ky) - I_0(kx) K_0(ky) \quad ,$$

where $I_0(x)$ and $K_0(x)$ are again modified Bessel functions. Also, for $\rho_i > \rho_j$ we find

$$E_r^{i>j}(\rho_i, \rho_j) = \frac{8\pi^2(\Delta r)\rho_j \sigma_j}{h^2} \sum_{n=1}^{\infty} \frac{n I_0(n\pi\rho_j/h)}{I_0(n\pi a/h)} \left[K_0\left(\frac{n\pi a}{h}\right) I_1\left(\frac{n\pi\rho_i}{h}\right) + I_0\left(\frac{n\pi a}{h}\right) K_1\left(\frac{n\pi\rho_i}{h}\right)\right] \sin^2\left(\frac{n\pi d}{h}\right) \quad . \tag{4}$$

The electric field acting on an electron in the ith ring from the other charge in the ith ring is found by assuming that σ is constant from $\rho - \Delta r/2$ to $\rho + \Delta r/2$. We find

$$\begin{aligned} E_r^{i=j}(\rho) = \frac{8\pi\sigma_j}{h} \sum_{n=1}^{\infty} \frac{\sin^2(n\pi d/h)}{I_0(n\pi a/h)} \Bigg\{ & -\left(\rho - \frac{\Delta r}{2}\right) I_1\left(\frac{n\pi}{h}\left(\rho - \frac{\Delta r}{2}\right)\right) \\ & \times \left[K_0\left(\frac{n\pi a}{h}\right) I_1\left(\frac{n\pi\rho}{h}\right) + I_0\left(\frac{n\pi a}{h}\right) K_1\left(\frac{n\pi\rho}{h}\right)\right] + \left(\rho + \frac{\Delta r}{2}\right) I_1\left(\frac{n\pi\rho}{h}\right) \\ & \times \left[I_1\left(\frac{n\pi}{h}\left(\rho + \frac{\Delta r}{2}\right)\right) K_0\left(\frac{n\pi a}{h}\right) + I_0\left(\frac{n\pi a}{h}\right) K_1\left(\frac{n\pi}{h}\left(\rho + \frac{\Delta r}{2}\right)\right)\right] \Bigg\} \quad . \end{aligned} \tag{5}$$

The charge density distribution for a given charge pool radius r is obtained by solving for σ_j the system of equations

$$\sum_{j=1}^{i-1} E_r^{i>j}(\rho_i, \rho_j) + E_r^{i=j}(\rho_i) + \sum_{j=i+1}^{j_{\max}} E_r^{i<j}(\rho_i, \rho_j) + E_r^{\text{bot}}(\rho_i) + E_r^{\text{top}}(\rho_i) = 0 \quad . \tag{6}$$

To obtain the charge density distribution as a function of charge pool radius r the above system of equations may be solved as $j_{\max}$ is decreased one ring at a time. The calculation is done for $V' = 0$ and for $V' = \Delta V$ where $0 < |\Delta V| << V$. The calculated $\sigma(\rho)$ for several values of r for a cell with the dimensions used in our experiment and for $d/h = 0.5$ is shown in Fig. 3. As a consequence of the finite element approximation used, the solution has oscillatory structure near the center of the charge pool. If $r = a$, so the charge pool covers the entire surface, the potential is constant on the surface. In this case σ is given explicitly by

$$\sigma(\rho, V) = -\frac{V}{4\pi d}\left[1 + \frac{2}{(s/d)} \sum_{n=1}^{\infty} \frac{(-1)^n \sin(n\pi s/d) I_0(n\pi\rho/d)}{n\pi I_0(n\pi a/d)}\right] \quad . \tag{7}$$

To obtain the charge density at the center of the charge pool we average $\sigma(\rho)$ from rings 3 to 8 (proceeding radially outward) of the 100 rings used in the numerical solution to Eq. (6) and renormalize so that when $r = a$ the result agrees with $\sigma(0)$ from Eq. (7).

Having found the surface charge density we next calculate the charge induced on the bottom plate by the surface charge. A ring with total charge q of radius ρ at the liquid surface is found to induce an amount q_b of charge on the bottom plate where

$$q_b(\rho)=2q\sum_{n=1}^{\infty}\frac{\sin(n\pi d/h)}{I_0(n\pi a/h)}\left\{I_0\left[\frac{n\pi a}{h}\right]I_0\left[\frac{n\pi\rho}{h}\right]\left[\left[\frac{a}{h}\right]K_1\left[\frac{n\pi a}{h}\right]-\left[\frac{b}{h}\right]K_1\left[\frac{n\pi\rho}{h}\right]\right]\right.$$
$$\left.+\left[\frac{a}{h}\right]I_0\left[\frac{n\pi\rho}{h}\right]K_0\left[\frac{n\pi a}{h}\right]I_1\left[\frac{n\pi a}{h}\right]-\left[\frac{\rho}{h}\right]I_0\left[\frac{n\pi a}{h}\right]K_0\left[\frac{n\pi\rho}{h}\right]I_1\left[\frac{n\pi\rho}{h}\right]\right\}. \quad (8)$$

The change in ac capacitance caused by free charge on the liquid surface is given by

$$\Delta C=\left.\frac{\partial Q_b}{\partial V'}\right|_{Q_s}. \quad (9)$$

Here Q_b is the total charge induced on the bottom plate by the free charge on the liquid surface and Q_s is the total free surface charge. Let Q_t be the total free charge induced on the top plate by the free charge on the liquid surface. One can use Green's reciprocation theorem with variation about nonzero V and zero V' to show[5] that

$$\left.\frac{\partial Q_b}{\partial V'}\right|_{Q_s}=\left.\frac{\partial Q_t}{\partial V}\right|_{Q_s}. \quad (10)$$

Hence, the ac capacitance is the same whether measured by changing the potential of the top plate and measuring the change in charge on the bottom plate or vice versa. Observe that ΔC would be zero if the surface charge did not move. One can also show that

$$\left.\frac{\partial Q_b}{\partial V'}\right|_{Q_s}=\left.\frac{\partial Q_b}{\partial V'}\right|_{r}-\left.\frac{\partial Q_s}{\partial V'}\right|_{r}\left.\frac{\partial Q_b}{\partial r}\right|_{V'}\left[\left.\frac{\partial Q_s}{\partial r}\right|_{V'}\right]^{-1}. \quad (11)$$

All of the quantities on the right-hand side (rhs) of Eq. (11) are known from our numerical calculation. In Fig. 2 we show that the measured capacitance is in excellent agreement with that calculated using Eq. (11).

To obtain the charge density at the center of the charge pool with bottom plate voltage V_2 from a measurement of $\Delta C/C$ with bottom plate voltage V_1 we make use of the fact that $\Delta C/C$ is a function of V/V_0 only, as mentioned earlier. Each value of $\Delta C/C$ and V_0/V corresponds to a unique charge pool radius r so $\Delta C/C=f_1(r)$ and $V_0/V=f_2(r)$. The ratio of $\sigma_r(\rho=0)$ when the charge pool has radius r to $\sigma_a(\rho=0)$ when the charge pool covers the surface (at fixed V) is independent of V and is used to define the function

$$\sigma_r(\rho=0)/\sigma_a(\rho=0)=f_3(r)$$

of r only. The value of $\sigma_a(\rho=0)$ when the charge pool covers the surface is given by Eq. (7), $\sigma_a(V)$. Our final result for the charge density near the center of the charge pool at cell voltage V_2 is

$$\sigma(\rho=0)=\sigma_a(V_2)f_3\left(f_2^{-1}\left(\frac{V_2}{V_1}f_2\left(f_1^{-1}\left(\frac{\Delta C}{C}\right)\right)\right)\right), \quad (12)$$

where the parentheses indicate the arguments of the functions f_1, etc. Knowing the charge density near the center of the charge pool we obtain the electric field acting on surface state electrons in a direction normal to the surface. In our experimental cell to a very good approximation the electric field is parallel to the cell axis near the center of the charge pool. Hence, the applied electric field acting on surface electrons near the axis is found by considering the analagous infinite parallel plate capacitor

$$E=\left\{\frac{V}{h}-\frac{4\pi\sigma}{1+\epsilon}\left[1-2\left[\frac{d}{h}\right]\right]\right\}\Big/\left[1-\frac{d}{h}\frac{(\epsilon-1)}{\epsilon}\right]. \quad (13)$$

Here ϵ is the dielectric constant of liquid helium.[6,7]

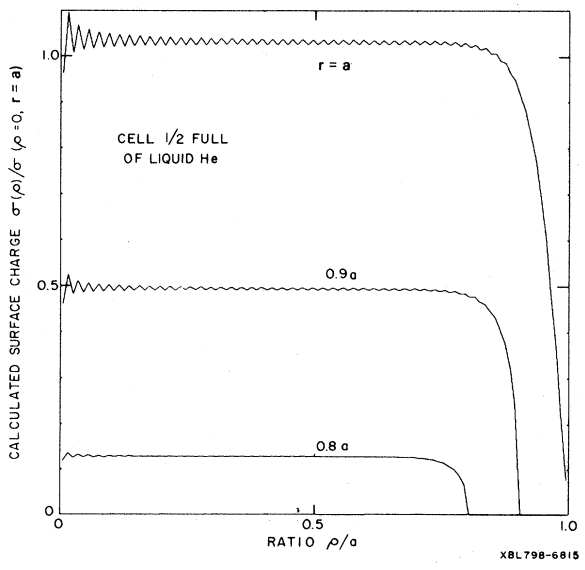

FIG. 3. Plot of the calculated surface charge density for several values of the charge pool radius (normalized to the surface charge density at the cell axis when the entire surface is covered with charge).

As mentioned previously we obtain d from the ac capacitance C_1 measured before liquid is put in the cell and C_2 after filling has stopped. Charge on the helium surface will press down on the helium surface and change d slightly. We find that to good approximation

$$d=\frac{\epsilon h}{\epsilon-1}\left(1-\frac{C_1}{C_2}\right)+\frac{E\sigma}{Dg}\left(\frac{A_2+A_3}{A_2+A_3+\pi r^2}\right)+\frac{(\epsilon-1)E^2A_3}{8\pi Dg(A_2+A_3+\pi r^2)}\,. \tag{14}$$

Here Dg is the product of the density of liquid helium with the acceleration of gravity, A_2 is the area of bulk liquid surface in the cell not covered by the charge pool, and A_3 is the area of liquid surface outside the cell. Under the conditions of our experiment the term of Eq. (14) proportional to E causes a change in d/h as large as order 10^{-3} while the term proportional to E_2 causes a change as large as order 10^{-4}.

We estimate our measurement of $\sigma(\rho=0)$ from Eq. (12) to be accurate to about 1%.

III. EXPERIMENTAL DETAILS

Our spectroscopic measurements are made by observing the transmission of radiation from a far-infrared laser through the cell to an InSb Rollin detector[8] as a function of cell voltage V. To obtain a satisfactory signal-to-noise ratio it is necessary to use modulation techniques. As shown in Fig. 4 the cell voltage is the sum of a linear ramp and a 60-kHz square wave. In addition, the optical signal from the laser is chopped at 100 Hz to make it possible to normalize out the effect of slow drifts in the output of the molecular laser. A slow feedback loop is used to ensure that the pump laser frequency remains near the peak of the gain curve of the molecular laser. Typically, a change in absorption of order 10^{-5} could be detected in one second.

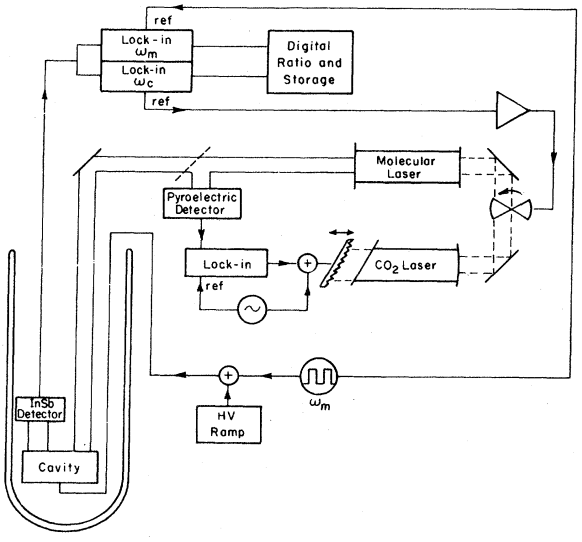

FIG. 4. Block diagram of the apparatus used for optical measurements.

The far-infrared source was a CH_3OH laser pumped by a CO_2 laser. The far-infrared laser lines were identified by approximate frequency measurements with a Martin-Puplett Fourier spectrometer.[9] The lasing frequency was then known to within a few Mhz (the width of the molecular laser gain curve) from the results of published heterodyne measurements. Although the molecular laser could be made to lase simultaneously at several widely spaced frequencies, this did not prove to be a problem in the measurement of narrow absorption lines. The frequencies used ranged from 428 to 765 GHz.

Measured values of the synchronous signal at the modulation frequency of the cell voltage and at the optical chopping frequency were recorded periodically by a computer. The linear ramp portion of the cell voltage was also sampled periodically. The ramp was repeated several times with different amplitudes of the cell voltage modulation. The optical transmission of the cell as a function of cell voltage was obtained from a numerical analysis of the data.

As mentioned previously, electrons are put on the liquid surface by briefly heating a small thoriated tungsten filament while a positive potential V relative to ground is applied to the bottom plate. To ensure that the charge pool does not flow off the liquid surface during a run it is important that V not be reduced below V_0 as discussed previously. If the charge pool is allowed to reach the walls the absorption lines are distorted and the shape of the CV curve is changed in an unreproducable way. Similar effects are observed if the Dewar is shaken or if the current through the filament is pulsed after the surface has previously been covered with charge. The Dewar is mounted on a vibration isolated table. The Dewar insert is adjusted so the top and bottom of the cell shown in Fig. 1 are parallel to the liquid-helium surface to within $\pm 2\times 10^{-4}$ rad. Parallelism is monitored by reflecting a He-Ne laser beam from a mirror attached to the Dewar insert and from the surface of a pool of water.

The homogeneous linewidth of the absorption lines has been investigated both theoretically,[10] and experimentally[2] and shown to decrease linearly with helium vapor pressure. For this reason, all of our data were measured at the lowest possible temperature in our cryostat which was about 1.2 K. It is found that the experimental line shape includes a contribution from the dispersion of the surface electron resonances as

well as the absorptive part. Radiation which has interacted with the surface electrons mixes in the detector with radiation which arrives directly from the laser. These effects are important because of the small size of the InSb hot electron bolometer ($1\times1\times2$ mm^3) and the coherence of the light from the laser. Similar effects are observed in NMR.[11] Because the relative phase shift of the interfering signals depends sensitively on the mode structure in the cell, the sign and magnitude of the dispersive contribution to the line shape changes from run to run.

IV. RESULTS

In order to discuss the spectroscopic measurements and the conclusions we have been able to draw from them, some background is necessary. We first describe a simple model for the electron-interface interaction which predicts the transition frequencies as a function of electric field in the limit of small surface charge density. We model the interaction with a one-dimensional potential in the z direction with a rise to infinite potential at $z=0$. For $z>0$ the Hamiltonian is

$$H=\frac{p^2}{2m}-\frac{(\epsilon-1)}{(\epsilon+1)}\frac{e^2}{4z}+eEz \quad . \tag{15}$$

The energy eigenvalues and corresponding eigenfunctions are obtained by numerically integrating Eq. (15) with the constraint that the wave function be square integrable and approach zero linearly in the limit that z approaches zero. In Fig. 5 we show that the transition frequencies from the ground state given by the model are in very close agreement with the measured transition frequencies extrapolated to zero surface charge. The small differences between the extrapolated measurements and the calculation are plotted in Fig. 6.

To extrapolate the measurements to zero surface charge density we used the theory given in a recent letter.[3] As explained there, the surface charge density dependence of the transition frequencies is small and arises because an excited state electron is acted upon by a nonzero average electric dipole field from nearby ground-state electrons. Explicitly, the change in applied external electric field needed to bring the 1-n transition back into resonance when the surface charge density is changed from zero to σ is

$$\Delta E=8.8927|\sigma|^{3/2}e^{-1/2}K(\Gamma)\times\left[(\langle z\rangle_n-\langle z\rangle_1)-\left[\frac{(\langle z^2\rangle_n-\langle z\rangle_n^2)-(\langle z^2\rangle_1-\langle z\rangle_1^2)}{2(\langle z\rangle_n-\langle z\rangle_1)}\right]\right] . \tag{16}$$

The factor in Eq. (16) containing various averages of z is obtained from the solution to Eq. (15). The rate of change with applied electric field of the transition energy between the ground state and the state n is

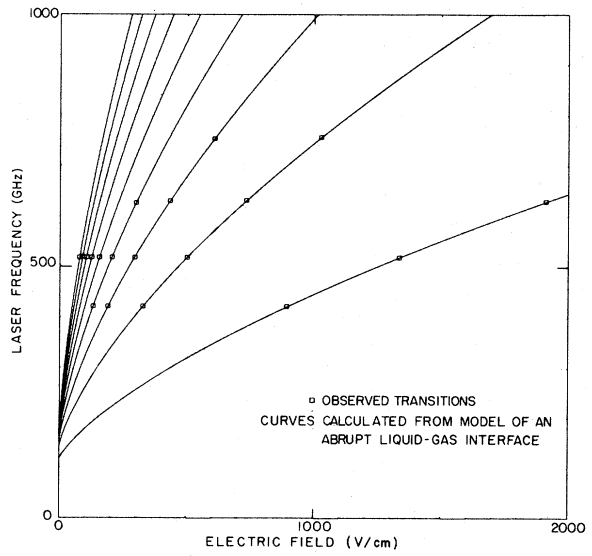

FIG. 5. Plot of transition frequencies vs applied electric field. The curves shown are obtained assuming an abrupt helium surface.

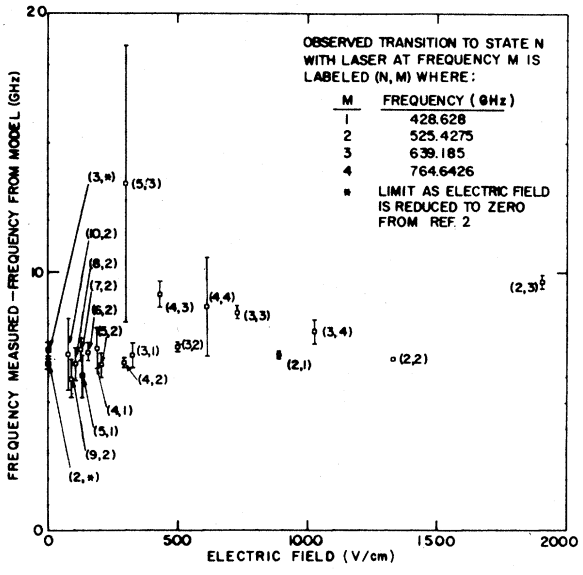

FIG. 6. Laser frequency for resonance (extrapolated to zero surface charge density) minus the frequency obtained assuming an abrupt helium surface, plotted as a function of external electric field. The error bars are $\pm\sigma_{\text{random}}$.

given by

$$\frac{dW_{1-n}}{dE} = e(\langle z\rangle_n - \langle z\rangle_1) \quad . \tag{17}$$

From Figs. 5 and 6 we see that the slope of the transition frequency versus the electric field predicted by the model differs very little from that of the actual measurements. Hence $\langle z\rangle_n - \langle z\rangle_1$ can be accurately obtained from the model. Also, the difference in the rms widths of the wave functions between the ground state and state n is small relative to $\langle z\rangle_n - \langle z\rangle_1$. The inaccuracy in ΔE introduced by using the model to obtain the averages of z is therefore expected to be about 1%.

We define a disorder parameter K which is the shift in the resonant frequency due to neighboring surface electrons normalized to the shift computed from a hexagonal lattice of surface electrons with the same average density. This K can be calculated from the radial charge distribution function as we discussed in a recent letter,[3] where a comparison was made between our data and published calculations.[12] It is expected to be a function of

$$\Gamma = \pi^{1/2} N_s^{1/2} e^2 / k_B T \quad ,$$

where N_s is the number density of surface electrons, k_B is Boltzman's constant, and T is the temperature. For the range of Γ used in our measurements, $9 < \Gamma < 44$, published theoretical results indicate that $1.06 < K < 1.20$. In our statistical analysis of the data we assumed that K was a constant independent of Γ. From this assumption we obtained $K = 1.114$ $(+0.096, -0.038)$. The experimentally determined value of K was then used to extrapolate our measurements back to zero surface charge density. The results are given in Table I.

The model we have used for the variation of potential near the liquid-vapor interface is very much oversimplified. A two-parameter model[13] due to Stern smooths out the unphysical discontinuity in the potential at $z = 0$. The values of the smoothing parameters he chose to give agreement with the data of Grimes *et al.*[12] yield transition frequencies shown in Fig. 7 which are consistent with our data at low electric fields. There do appear to be significant differences at high electric fields for the 1-2 transition, however.

In addition to comparing our measurements with the transition frequencies predicted by a one-dimensional model potential it would be very interesting to compare them with the results of first-principles calculations. In recent years a number of such calculations for the surface tension and density variation near the liquid-vapor interface of ^{4}He have appeared.[14–21] Although all calculations seem to be consistent with the measured surface tension, other

TABLE. I. Observed values of the applied electric field for various transitions and laser frequencies extrapolated to zero surface charge density. The quoted statistical error ($\pm\sigma$) does not include a systematic error from our uncertainty in h of $5.7 \times 10^{-4} E$.

Transition	Laser frequency (GHz)	E (V/cm)
1-2	428.63	895.89 (0.66)
1-3	428.63	329.13 (0.80)
1-4	428.63	191.57 (0.78)
1-5	428.63	133.09 (0.61)
1-2	525.43	1336.39 (0.39)
1-3	525.43	502.81 (0.37)
1-4	525.43	296.04 (0.22)
1-5	525.43	206.76 (0.40)
1-6	525.43	157.72 (0.22)
1-7	525.43	127.28 (0.22)
1-8	525.43	106.62 (0.27)
1-9	525.43	91.76 (0.27)
1-10	525.43	80.00 (0.46)
1-2	639.19	1913.18 (1.41)
1-3	639.19	735.71 (0.54)
1-4	639.19	435.65 (0.68)
1-5	639.19	301.24 (5.03)
1-3	764.64	1029.55 (1.18)
1-4	764.64	609.53 (2.88)

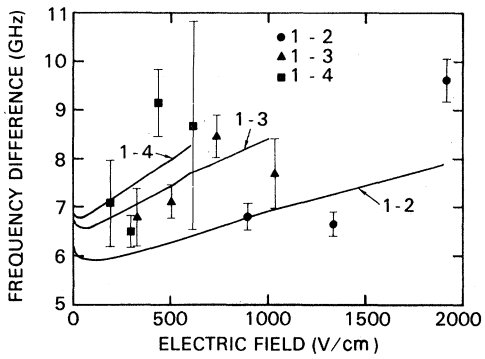

FIG. 7. Comparison of the transition frequencies calculated from the model proposed by Stern with the measured transition frequencies (extrapolated to zero surface charge density). In both cases the calculated or measured frequency minus the frequency calculated from the model of an abrupt helium surface is plotted. The curves are from Stern's model and the experimental error bars are $\pm(\sigma_{\text{random}}+\sigma_{\text{systematic}})$. The errors in the theoretical calculation are believed to be less than 0.2 GHz.

aspects of their results appear to be quite different. In particular, the surface tension found by Ebner and Saam[21] using density functional theory is almost exclusively due to the zero-point motion of surface modes (ripplons) while in quantum many-body calculations the ripplons are neglected and the surface tension arises from the rapid variation of the wave function normal to the surface. Also, the length over which the density varies from liquid to vapor varies greatly between the calculations and some find oscillations in the density near the surface. It would be very useful if these calculations were extended so that they can be compared with our measurements.[22]

It should be mentioned that the reflection of ^{4}He atoms from the ^{4}He liquid surface has been measured.[23] A model of Echenique and Pendry[24] explains the observed smallness of the reflectivity if the helium density changes from its liquid to vapor density over a distance of at least 5 Å. Ellipsometric measurements[25] are probably possible as well.

V. CONCLUSION

Our CV measurement technique makes it possible to obtain accurate measurements of both the surface charge density and the external electric field applied to electrons near the axis of our absorption cell. Using this technique, we have measured transition frequencies of electrons on the surface of liquid helium which are subjected to large electric fields. The surface charge density dependence of the resonance condition was shown in a recent letter[3] to provide a way to obtain the local disorder in the 2D electron gas. The zero-surface-charge-density limit of the transition frequencies when large external electric fields are applied has also been obtained. The slope of measured curves of transition frequency versus electric field is in close agreement with a simple model—showing that the model accurately predicts the change in the average distance of the surface electron from the surface when a transition occurs. Good agreement is found between our measurements and a one-dimensional model potential calculation of Stern. Our measurements could also help verify which of the conflicting calculations of density variation near a helium liquid-vapor interface is closest to being correct.

ACKNOWLEDGMENTS

We are indebted to Dr. C. C. Grimes who provided the filament material and many useful suggestions. Helpful conversations with Dr. F. Stern and Dr. J. Lekner are also acknowledged. One of us (D.L.) would like to express gratitude for an IBM fellowship. This work was performed under the auspices of the U.S. Department of Energy under Contract No. W-7405-ENG-48.

*Present address: Physics Dept., Research Laboratories, General Motors Corporation, Warren, Mich. 48090.

[1]C. C. Grimes, Surf. Sci. 73, 379 (1978).
[2]C. C. Grimes, T. R. Brown, M. L. Burns, and C. L. Zipfel, Phys. Rev. B 13, 140 (1976).
[3]D. K. Lambert and P. L. Richards, Phys. Rev. Lett. 44, 1427 (1980).
[4]C. L. Zipfel, T. R. Brown, and C. C. Grimes, Surf. Sci. 58, 283 (1976).
[5]D. K. Lambert, Lawrence Berkeley Laboratory Report LBL-9553 (unpublished), p. 97.
[6]R. F. Harris-Lowe and K. A. Smee, Phys. Rev. A 2, 158 (1970).
[7]C. Van Degrift, thesis (University of California, Irvine, 1974) (unpublished).
[8]E. H. Putley, in *Semiconductors and Semimetals*, edited by R. K. Willardson and A. C. Beer (Academic, New York, 1977), Vol. 12, Chap. 3, pp. 143–168.
[9]D. K. Lambert and P. L. Richards, Appl. Opt. 17, 1595 (1978).
[10]T. Ando, J. Phys. Soc. Jpn. 44, 765 (1978).
[11]A. Abragam, *The Principles of Nuclear Magnetism* (Oxford, London, 1961), p. 76.
[12]In addition to the references given in Ref. 3, see also N. Itoh, S. Ichimaru, and S. Nagano, Phys. Rev. B 17, 2862 (1978).

[13]F. Stern, Phys. Rev. B 17, 5009 (1978); and private communication.
[14]T. Regge, J. Low Temp. Phys. 9, 123 (1972).
[15]R. M. Bowley, J. Phys. C 3, 2012 (1970).
[16]Y. M. Shih and C.-W. Woo, Phys. Rev. Lett. 30, 479 (1973); L. A. Wojick, Y. M. Shih, and C.-W. Woo, J. Low Temp. Phys. 23, 345 (1976).
[17]F. D. Mackie and C.-W. Woo, Phys. Rev. A 18, 529 (1978).
[18]C. C. Chang and M. H. Cohen, Phys. Rev. A 8, 1930 (1973).
[19]K. S. Liu, H. M. Kalos, and G. V. Chester, Phys. Rev. B 12, 1715 (1975).
[20]T. C. Padmore and M. W. Cole, Phys. Rev. A 9, 802 (1974).
[21]C. Ebner and W. F. Saam, Phys. Rev. B 12, 923 (1975).
[22]H. -M. Huang, Y. M. Shih, and C.-W. Woo, J. Low Temp. Phys. 14, 413 (1974). The frequency difference between the result of this calculation and the abrupt interface model is a factor of 3 greater than that measured.
[23]D. O. Edwards, J. R. Eckardt, and F. M. Gasparini, Phys. Rev. A 9, 2070 (1974).
[24]P. M. Echenique and J. B. Pendry, Phys. Rev. Lett. 37, 561 (1976).
[25]D. Beaglehole, Phys. Rev. Lett. 43, 2016 (1979).